Modelling and Evaluating Capability of Battery Storage Systems to Provide Extreme Event Services to the DSO: Case Study of Croatia

Bojana Barać, Matija Kostelac,
Ivan Pavić, Tomislav Capuder
Department of Energy and Power Systems
University of Zagreb Faculty of Electrical Engineering and Computing, Zagreb, Croatia
{bojana.barac, matija.kostelac, ivan.pavic, tomislav.capuder}@fer.hr

Joško Grašo, Anton Marušić,
Tomislav Koledić, Josipa Barišin
HEP DSO Ltd.
Elektra Zagreb, Croatia
{josko.graso, anton.marusic, tomislav.koledic, josipa.barisin}@hep.hr

***Abstract*—The City of Zagreb in Croatia and its surroundings have experienced two strong earthquakes within nine months of 2020. Putting this in the context of the increased workload of healthcare facilities due to Covid-19, the distribution system operator (DSO) is encouraged to look for unconventional solutions such as integrating the battery energy storage system (BESS) to supply healthcare facilities during network fault conditions or other extreme network events. The BESS size and location are determined by optimization model, while the control system of the BESS converter, based on the virtual synchronous machine (VSM) concept, is define to test BESS ability to supply critical consumers in the off-grid mode. The models are tested and verified on several real world situations in Zagreb MV distribution network. Future developments and scenarios are also simulated to verify the robustness of the proposed investment.**

***Index Terms*—battery energy storage system (BESS), dynamic model, dynamic stability, islanded operation, microgrid system, optimization model**

I. Introduction

With newly defined pathways for limiting global warming, the power system experiences the transition from a centralised and carbon-based system with a passive distribution grid to a decentralized, low-carbon system with an active distribution grid. By development and advancement of the energy storage technologies, and their importance to achieve the decarbonization of the energy sector, the price of energy storage systems has decreased. The applications of the battery energy storage system (BESS) have increased, since BESS can support the grid by providing local and global ancillary services [1]. BESS can enhance the power system flexibility and enable greater integration of the renewable energy sources (RES) [2], [3]. Due to its ability to rapidly charge or discharge in a second, the BESS can provide the primary frequency response and regulation, faster than a conventional generator [2], [4]. Although they are usually used for short-term reliability services, appropriately sized BESS can also provide longer-duration services, i.e. meet demand in islanded systems [2]. The BESS has also other purposes, such as: voltage support [5], energy arbitrage [6], firm capacity or peak capacity, black start, and transmission and distribution upgrade deferrals [2]. To provide the mentioned ancillary services, the BESS require the appropriate converter control system. The BESS is commonly interfaced to the grid via grid-following converters that are designed to inject active and reactive power during grid-connected operation [7]. For independent operation in an islanded system, the BESS requires the grid-forming converter that has the ability to set frequency and voltage references [7].

In addition to the control system, the BESS ability to provide ancillary services is determined by its location and size. The BESS is commonly placed in the transmission network, or distribution network near load centers, or co-located with variable RES [2]. To ensure the resilient and economic operation of the network, the BESS size and location should be optimized [8]. The undersized BESS may not provide expected services, while the oversized BESS causes unnecessary additional costs [8]. The unsuitable BESS location and size can also cause low or over-voltages in the distribution network [3]. Furthermore, the BESS location and size should be co-optimized, since an inappropriately sized BESS, installed at the optimal location, increases the voltage or power flow violations [3]. Additionally, the grid application requirements have to be considered during the optimization. The sizing of the BESS for frequency control and peak shaving is presented by multi-objective approach in [1]. The optimization of the BESS size and location, in order to balance voltage violations in a distribution grid with high photovoltaic (PV) penetration, is shown in [9].

This paper presents an analysis of the BESS integration into the distribution network in Zagreb, Croatia. The main idea ia to install BESS of enough capacity and power to supply significant consumers (healthcare facilities) during fault conditions in the distribution network. Two strong earthquakes in Zagreb and its surroundings within nine months of 2020 and heavier workload of the healthcare facilities due to Covid-19, as well as their additional sensitivity to electricity loss, were incentives

to enhance system security. Therefore, it is necessary to ensure the provision of ancillary services of the BESS during off-grid transition and operation. Firstly, the optimal size and location of the BESS are defined with the aim of the cost minimization and the maximization of energy supplied from the battery. Then, the dynamic models of the BESS and its converter system are developed, enabling the stable off-grid transition and operation. To determine dynamic islanding constraints of the installed BESS, the specific simulation examples are executed. The main contribution of this paper is the real-world case of the BESS dimensioning for islanded operation including: i) optimization model that ensures the BESS can transition to an islanding mode and maintain supply for 3 hours as defined by the DSO and ii) dynamic model based on the existing *Virtual Synchronous Machine* (VSM) model, but expanded with the DC side dynamics.

Rest of the paper is organized as follows: Section II presents the optimization and dynamic models; results of specific case studies are given in Section III; some future scenarios are presented in Section IV; Section V concludes the paper.

II. System Modelling

The observed distribution network (10 and 0,4 kV) is part of the Croatian power system, and it is shown in Fig. 1. The macro location analysis has suggested the installation of BESS near the significant consumers, primary the hospitals, as they are sensitive to electricity loss. In Fig. 1, the significant consumers are marked with L1 - L8. They are modelled as passive loads and their power consumption is based on the real measurements on this location. All the significant consumers are located at three distribution circuits, shown in different colors in Fig. 1. These circuits are considered as microgrids during BESS sizing. Therefore, the four microgrids are defined for analysis purposes: 1^{st} microgrid (shown in blue), 2^{nd} microgrid (shown in red), 3^{rd} microgrid (shown in green), and 4^{th} microgrid (all three together).

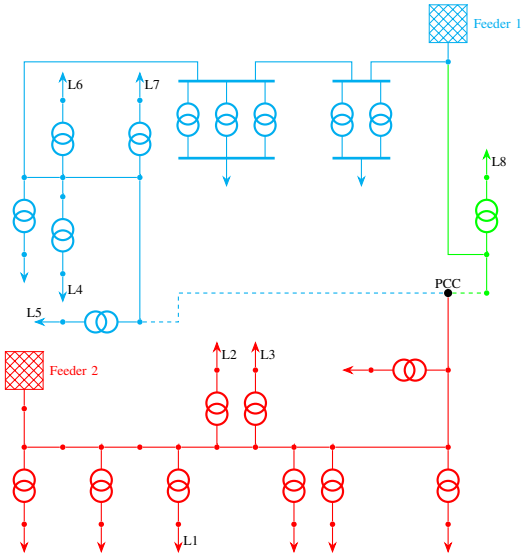

Fig. 1: Layout of the observed microgrids

A. BESS sizing and placement

The aim of the optimization model is to determine the optimal size of BESS that is suitable to supply all significant consumers within the observed microgrid for 3 hours. The optimization time step is 15 minute interval. For optimization purposes, the 8 characteristic days are chosen, two days for each season. Only the consumption of significant consumers is considered, while the consumption of other consumers is not observed (their consumption is set to 0).

The objective function of this optimization problem is to minimize the costs caused by network operating losses and battery investment costs. It is given by (1):

$$min \sum_{t} \sum_{ik \in L} R_{ik} \cdot l_{ik,t} \cdot c_{loss} + C_{bat} \cdot c_1 + S_{bat,max} \cdot c_2 \quad (1)$$

where L presents all lines of the observed microgrid, R_{ik} is the line resistance, $l_{ik,t}$ is the square value of the current of the line ik at the moment t, c_{loss} is the price for power losses, C_{bat} is the battery capacity, $S_{bat,max}$ is the battery maximum rated power, c_1 is price per battery capacity unit, c_2 is the price per battery power unit. The BESS is defined by its capacity at any moment. The battery capacity has to be within its defined minimum and maximum value. The maximum charge and discharge powers are limited with the BESS maximum active power, and the reactive power flow is limited with the maximum reactive power of the converter. Also, the total active and reactive power can not be bigger than the apparent rated power. Furthermore, the optimization model involves the optimal power flow (OPF) problem. The goal of the OPF problem is to find the optimal power grid settings that optimize the objective function, satisfying the power flow equations, system security, and operating limitations of the grid components [10]. The *DistFlow* is used to describe the power flow in the distribution networks [11]. However, the OPF problem is hard to solve due to nonlinear power flows. Therefore, the *Second-order cone programming* (SOCP) is applied to the OPF problem, enabling the quick solving of the optimization problem and finding the global optimum [12]. When solving the BESS placement, a binary variable x_{bat} is included in the power flow equations and represents which node has a BESS installed. x_{bat} is defined for each node of microgrid, but only in one node can take the value 1, i.e. $\sum_{i \in N} x_{bat,i} = 1$. In this way, the node that contributes most to the objective function is selected. The optimization model is only briefly described to understand the choice of BESS size and location, which play an important role in dynamic analysis.

B. Dynamic model

All microgrids with the associated BESS control system are modelled in DIgSILENT PowerFactory 2019. When connecting the BESS, it is necessary to ensure the ancillary services provision and dynamically stable off-grid transition and operation. Therefore, the VSM is used, whose technology is designed to mimic characteristics of the synchronous generator (SG) [13]. VSM is a grid-forming converter with the

ability to provide virtual inertia and set frequency and voltage references. The control scheme of the BESS converter, shown in Fig. 2, is based on [13].

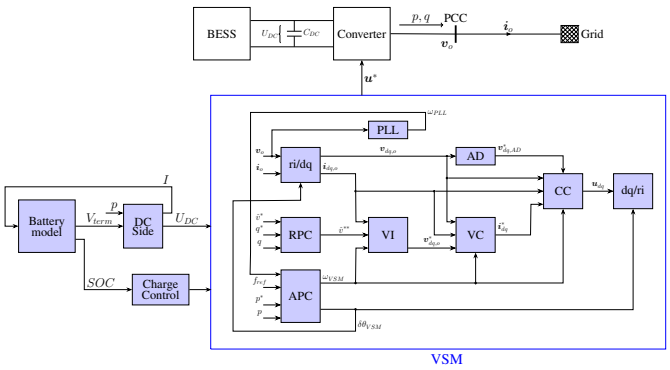

Fig. 2: Dynamic model of the BESS

The battery model block is based on the available model in PowerFactory, and it is described in [14].

The DC side voltage and DC current are calculated by (2) and (3), respectively, where P is the measured active power in MW.

$$\frac{dU_{DC}}{dt} = \frac{V_{term} - U_{DC}}{0,01} \tag{2}$$

$$I = \frac{P \cdot 10^3}{U_{DC}} \tag{3}$$

The VSM control system is modelled in the *dq* synchronous reference frame. Therefore, the measured voltage and current have to be transformed from the global (grid) reference frame to the VSM reference frame, as shown by (4):

$$\boldsymbol{v}_{dq,o} = (v_{r,o} + jv_{i,o}) \cdot e^{-j\delta\theta_{VSM}} \tag{4}$$

where $v_{r,o}$ and $v_{i,o}$ are real and imaginary components of the measured voltage, and $\delta\theta_{VSM}$ presents the phase displacement between reference frames. The measured current is transformed analogously.

The block of the virtual inertia and active power control (APC) enables the BESS frequency response, and emulation of the inertia and damping effect of the SG. Its implementation is based on a swing equation that is linearized with respect to the angular speed, as shown by (5):

$$\frac{d\omega_{VSM}}{dt} = \frac{1}{T_a}\Big(p^* - p - k_d(\omega_{VSM} - \omega_{PLL}) - k_\omega(\omega_{VSM} - \omega^*_{VSM})\Big) \tag{5}$$

where ω_{VSM} is the VSM angular speed; p^* is the external power reference; p is the BESS output electrical power flowing to the microgrid; T_a is the mechanical time constant that corresponds to $2H$ in a traditional SG; ω_{PLL} is the grid frequency estimated by a phase locked loop (PLL) whose implementation is available in the PowerFactory library; k_d is the damping constant; k_ω is the droop constant; ω^*_{VSM} is the reference VSM frequency. The VSM phase displacement is calculated by (6):

$$\frac{d\delta\theta_{VSM}}{dt} = \delta\omega_{VSM} \cdot \omega_b \tag{6}$$

where ω_b corresponds to $2\pi 50$, and $\delta\omega_{VSM} = \omega_{VSM} - f_{ref}$.

The reactive power controller (RPC) outputs the voltage amplitude reference v^{**}, as given by (7):

$$v^{**} = v^* + k_q(q^* - \hat{q}) \tag{7}$$

$$\frac{d\hat{q}}{dt} = -\omega_f \cdot \hat{q} + \omega_f \cdot q \tag{8}$$

where v^* is the external voltage amplitude reference, q^* is the reactive power reference, k_q is the reactive power droop gain, $\hat{q}$ is the filtered value of the measured reactive power q (8). The voltage amplitude reference is the input signal to the cascaded voltage and current control loops.

Due to high R/X ratio in the distribution networks, the active and reactive power flows are coupled. Therefore, the voltage amplitude reference is firstly passed through the block of virtual impedance (VI), as shown by (9) and (10):

$$v^*_{d,o} = v^{**} - r_v \cdot i_{d,o} + \omega_{VSM} \cdot l_v \cdot i_{q,o} \tag{9}$$

$$v^*_{q,o} = 0 - r_v \cdot i_{q,o} - \omega_{VSM} \cdot l_v \cdot i_{d,o} \tag{10}$$

where r_v and l_v are virtual resistance and inductance.

The cascade of the voltage (VC) and current control (CC) loops is designed as it is usual for grid-forming converters. Their implementation is presented by (11) and (13). The states of the voltage PI controllers and the current PI controllers are given by (12) and (14), respectively; where k_{pv}, k_{iv}, k_{pc} and k_{ic} are the respected PI controller gains.

$$\boldsymbol{i}^*_{dq,o} = k_{pv}(\boldsymbol{v}^*_{dq,o} - \boldsymbol{v}_{dq,o}) + k_{iv}\boldsymbol{\epsilon} + k_{ffi} \cdot \boldsymbol{i}_{dq,o} \tag{11}$$

$$\frac{d\boldsymbol{\epsilon}}{dt} = \boldsymbol{v}^*_{dq,o} - \boldsymbol{v}_{dq,o} \tag{12}$$

$$\boldsymbol{v}_{dq,CV} = k_{pc}(\boldsymbol{i}^*_{dq,o} - \boldsymbol{i}_{dq,o}) + k_{ic}\boldsymbol{\gamma} + k_{ffv} \cdot \boldsymbol{v}_{dq,o} - \boldsymbol{v}^*_{dq,AD} \tag{13}$$

$$\frac{d\boldsymbol{\gamma}}{dt} = \boldsymbol{i}^*_{dq,o} - \boldsymbol{i}_{dq,o} \tag{14}$$

$\boldsymbol{v}^*_{dq,AD}$ is the output signal of the active damping (AD) block used to remove the oscillations of the measured voltage $\boldsymbol{v}_{dq,o}$. The converter voltage reference $\boldsymbol{v}_{dq,CV}$ is divided with the DC side voltage U_{DC} to generate the modulation signals used to manage the converter. It is also necessary to return the modulation signals to the global reference frame using the rotation by $e^{j\delta\theta_{VSM}}$.

Since the battery has ability to charge and discharge, the charge control is important to check whether the active component (d-component) of current and SOC are within certain limits. The battery charging is disabled if the SOC is above a certain value ($maxSOC$), while the battery discharging is disabled if the SOC is below a certain value ($minSOC$).

III. Dynamic simulations and results

Depending on the results of the optimization model from Section II-A, the BESS of appropriate power and capacity is connected to each microgrid. Optimization results are given in Table I. The optimal location for all microgrids is node PCC (see Fig. 1), i.e. the intersection of three distribution circuits.

TABLE I: Optimization results

Microgrid	Active power [MW]	Apparent power [MVA]	Capacity [MWh]
1^{st}	0.629	0.663	2.456
2^{nd}	0.931	0.98	3.588
3^{rd}	0.203	0.228	0.786
4^{th}	1.754	1.846	6.893

For each of four microgrids, the islanding is triggered at $t = 4$ s. It is scrutinized whether the microgrids achieve stable off-grid transition and operation for two operating points, the maximum and minimum microgrid load. For each microgrid and for each operating point, three case studies are analyzed: i) BESS does not charge nor discharge before islanding, ii) BESS charges with maximum active power before islanding and iii) BESS discharges with maximum active power before islanding. 1^{st} and 3^{rd} microgrids are supplied by Feeder 1, while 2^{nd} is supplied by Feeder 2 before islanding. In 4^{th} microgrid, the BESS is connected to the red circuit before islanding. When islanding occurs, the blue and green circuits connect to PCC, but considering a time delay of protection relays and circuit breakers (45 - 70 ms [15]). The total time delay is assumed to be 150 ms, according to engineering practice.

The microgrid can achieve the stable off-grid transition and operation if the following is satisfied: the steady-state is reached, bus voltages are within $\pm$ 10 % of nominal value, and frequency is within $\pm$ 2 Hz in the first second after an islanding after which it is within $\pm$ 1 Hz [14].

Plots of results are omitted for brevity if the constraints are met. Plots present the frequency and voltage measured at the PCC.

A. Case I: BESS does not charge nor discharge before islanding

In this case, the off-grid transition of all microgrids for both operating points is feasible, i.e. the frequency and voltage limits are satisfied.

B. Case II: BESS charges with maximum active power before islanding

This case is feasible only for off-grid transition during minimum microgrid load. Otherwise, it is as follows:

1) 1^{st} *microgrid*: When the microgrid load is maximal before islanding, the frequency constraints are not met, as shown in Fig. 3a. In order to achieve a stable off-grid transition, the BESS has to be charged with a maximum active power of 0.255 MW before islanding.

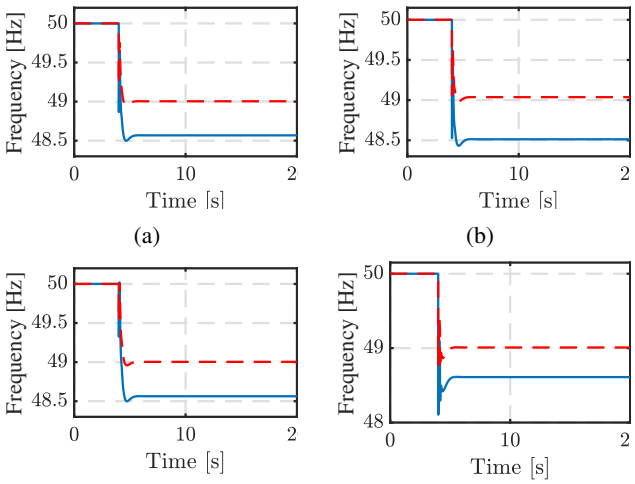

Fig. 3: Case II frequency for [blue - without limitation; red - with limitation]: (a) 1^{st} microgrid, (b) 2^{nd} microgrid, (c) 3^{rd} microgrid, (d) 4^{th} microgrid

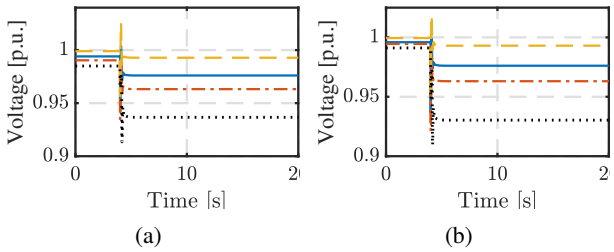

Fig. 4: Case II voltage: (a) without limitation; (b) with limitation

2) 2^{nd} *microgrid*: The frequency constraints are not met when the microgrid load is on its maximum before islanding, as shown in Fig. 3b. Therefore, the maximum charge power is limited to 0.3 MW.

3) 3^{rd} *microgrid*: The frequency constraints are not satisfied when the islanding occurs during the maximum microgrid load, as shown in Fig. 3c. The only way to achieve a stable off-grid transition is to limit the maximum charge power to 0.0725 MW.

4) 4^{th} *microgrid*: During the maximum microgrid load, this case is unfeasible, as shown in Fig. 3d. In order to satisfy the frequency constraints and achieve stable off-grid transition, the maximum charge power is limited to 0.825 MW.

The voltage constraints are met for all microgrids, as shown in Fig. 4.

C. Case III: BESS discharges with maximum active power before islanding

When the BESS discharges with maximum active power before islanding, all microgrids can achieve stable off-grid transition for both operating points.

The power constraints of the BESS, determined by dynamic analysis, are then involved in the initial optimization problem to ensure minimal operational cost while meeting constraints for dynamic stability.

IV. Expected future scenarios

In this section, the stability of the 4^{th} microgrid during transition to islanded mode is checked, but for some possible future scenarios.

One of the possible scenarios is the increase in the microgrid load. The increase of 30 % is assumed. The most challenging case is transition to islanded mode during maximum microgrid load and BESS charging. As shown in Fig. 5, the frequency and voltage limitations are not satisfied, due to microgrid overload.

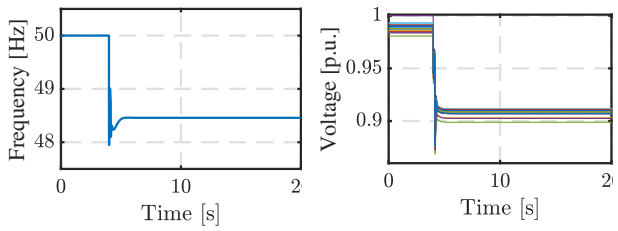

(a) (b)

Fig. 5: Results for increase in microgrid load: (a) Frequency; (b) Terminal voltages

The next assumed scenario is the RES integration into 4^{th} microgrid. Hence, the PV unit of 2.5 MVA is connected within observed microgrid. The most challenging case is islanding during minimum microgrid load and BESS discharging. As shown in Fig. 6, the frequency and voltage deviations are greater than allowed, due to microgrid underload.

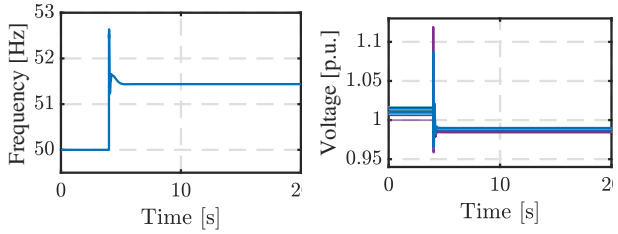

(a) (b)

Fig. 6: Results for PV integration: (a) Frequency; (b) Terminal voltages

V. Conclusion

Two earthquakes, which happened in the City of Zagreb and its surroundings, as well as the Covid-19 pandemic, have shown insecurity in the supply of healthcare facilities. Hence, the distribution system operator (DSO) looks for the application of the battery storage system (BESS) near healthcare facilities. The observed consumers are placed at three distribution circuits. The BESS size and location are determined by an optimization model with the aim of costs minimization and use maximization. The intersection of circuits is determined as a BESS optimal location, and the BESS has the ability to supply each of them or all three together. Furthermore, a virtual synchronous machine (VSM) is applied to the BESS converter to achieve dynamically stable off-grid transition and operation. Then, specific simulations are executed to determine dynamic constraints in the islanded mode for three specific cases. The results show infeasible off-grid transition only when the BESS charges with the maximum active power before islanding and the microgrid load is maximal.

Acknowledgment

This work was supported by the Croatian Science Foundation and European Union through the European Social Fund under the project Flexibility of Converter-based Microgrids–FLEXIBASE (PZS-2019-02-7747), as well as the Croatian Science Foundation and Croatian Distribution System Operator (HEP ODS) under the project Innovative Modelling and Laboratory Tested Solutions for Next Generation of Distribution Networks–IMAGINE (PAR-2018-12). Employment of Bojana Barać is fully funded by the Croatian Science Foundation within programme DOK-2021-02.

References

[1] N. B. Arias, J. C. López, S. Hashemi, J. F. Franco, and M. J. Rider, "Multi-objective sizing of battery energy storage systems for stackable grid applications," *IEEE Transactions on Smart Grid*, vol. 12, no. 3, pp. 2708–2721, 2020.

[2] T. Bowen, I. Chernyakhovskiy, and P. L. Denholm, "Grid-scale battery storage: frequently asked questions," National Renewable Energy Lab.(NREL), Golden, CO (United States), Tech. Rep., 2019.

[3] S. B. Karanki, D. Xu, B. Venkatesh, and B. N. Singh, "Optimal location of battery energy storage systems in power distribution network for integrating renewable energy sources," in *2013 IEEE Energy Conversion Congress and Exposition*. IEEE, 2013, pp. 4553–4558.

[4] H.-S. Kim, J. Hong, and I.-S. Choi, "Implementation of distributed autonomous control based battery energy storage system for frequency regulation," *Energies*, vol. 14, no. 9, p. 2672, 2021.

[5] F. Marra, Y. T. Fawzy, T. Bülo, and B. Blažic, "Energy storage options for voltage support in low-voltage grids with high penetration of photovoltaic," in *2012 3rd IEEE PES Innovative Smart Grid Technologies Europe (ISGT Europe)*. IEEE, 2012, pp. 1–7.

[6] C. Brivio, S. Mandelli, and M. Merlo, "Battery energy storage system for primary control reserve and energy arbitrage," *Sustainable Energy, Grids and Networks*, vol. 6, pp. 152–165, 2016.

[7] J. Rocabert, A. Luna, F. Blaabjerg, and P. Rodriguez, "Control of power converters in ac microgrids," *IEEE transactions on power electronics*, vol. 27, no. 11, pp. 4734–4749, 2012.

[8] M. Hannan, M. Faisal, P. J. Ker, R. Begum, Z. Dong, and C. Zhang, "Review of optimal methods and algorithms for sizing energy storage systems to achieve decarbonization in microgrid applications," *Renewable and Sustainable Energy Reviews*, vol. 131, p. 110022, 2020.

[9] B. Matthiss, A. Momenifarahani, and J. Binder, "Storage placement and sizing in a distribution grid with high pv generation," *Energies*, vol. 14, no. 2, p. 303, 2021.

[10] J. Zhu, "Optimization of power system operation, a john wiley & sons," *Inc. Publication, IEEE*, 2009.

[11] M. E. Baran and F. F. Wu, "Optimal capacitor placement on radial distribution systems," *IEEE Transactions on power Delivery*, vol. 4, no. 1, pp. 725–734, 1989.

[12] S. Bansal and C.-Y. Shih, "Convex relaxation of optimal power flow problem," *Project Report, UC Berkeley.[Online]. Available: https://people. eecs. berkeley. edu/somil/Papers/project report. pdf.*

[13] S. D'Arco, J. A. Suul, and O. B. Fosso, "A virtual synchronous machine implementation for distributed control of power converters in smartgrids," *Electric Power Systems Research*, vol. 122, pp. 180–197, 2015.

[14] T. Capuder, M. Kostelac, M. Krpan, and I. Pavić, "Multi-energy microgrid ability to provide flexibility services to the system operator and security of supply to end-users," in *2020 International Conference on Smart Energy Systems and Technologies (SEST)*. IEEE, 2020, pp. 1–6.

[15] "VD4/R MV vacuum circuit breakers for secondary distribution," 2018.